JOURNAL OF MATERIALS SCIENCE 23 (1988) 934–940

The coincident axial direction (CAD) approach to grain boundary structure

VALERIE RANDLE, BRIAN RALPH
Department of Materials Technology, Brunel University of West London, Uxbridge, Middlesex, UB8 3PH, UK

A report is presented which describes grain boundary geometry in terms of the near parallelism of plane stack normals in neighbouring grains. Boundaries whose axes of rotation are within a certain angular limit of low-index directions are called coincident axial direction (CAD) boundaries. It is demonstrated that the CAD model is a special case of the coincident-site lattice (CSL) model, and can be applied in an analogous manner. Data from five different materials are analysed using the CAD theory and the overall fraction of boundaries corresponding to a CAD description is 63 to 76% for CAD axes $\langle h\,k\,l \rangle$ having $\Pi < 24$ where $\Pi = h^2 + k^2 + l^2$. Some of the data are analysed in more detail in the light of the interrelationships between microtexture, grain misorientation texture (GMT), CSL and CAD distributions. It is clear that often these distributions are non-random. Finally, it is suggested that the high proportion of boundaries found to possess CAD structures lends support to the hypothesis that few boundaries are totally disordered, which may have a consequent effect on the structure-sensitive properties of grain boundaries.

1. Introduction

"Special" grain boundaries are characterized by a periodic structure which may be described in terms of dislocations, ledges or repeating atomic groups at the interface. Those boundaries which are two-dimensionally periodic in the boundary plane are accounted for by the coincident-site lattice (CSL) theory and variants of it. Although the extent to which secondary intrinsic dislocation arrays are capable of maintaining the coincidence structure has no rigourously defined limit [1], by analogy with the low-angle boundary case the deviation v depends upon both the Burgers vector $\boldsymbol{b}$ and the network spacing h:

$$v \propto \boldsymbol{b}/h \tag{1}$$

The planar matching (PM) theory was initiated to explain the observation of intrinsic dislocations in boundaries which were outside the range commonly accepted for categorization by a CSL description. The basic concept of the PM theory is that some atomic planes from each grain may be only slightly misaligned across the boundary. These planes may then relax to regions of perfect matching in the boundary plane, interspersed with lines of mismatch which are evident as arrays of intrinsic dislocations analogous to the interphase semicoherent interface case [2, 3]. The essential difference between the CSL and PM models is that the former predicts three-dimensional lattice matching while the latter is only concerned with linear (one-dimensional) matching. However, the observation of one or more sets of grain boundary defects in the transmission electron microscope (TEM) is not in itself sufficient evidence that the boundary is a PM type rather than CSL, since other dislocation arrays may be present but too closely spaced to be resolvable in the TEM.

Planar matching can alternatively but equivalently be considered from the standpoint of the deviation from parallelism of the plane stack normals, rather than the misorientations across the planes themselves. In other words, the angular deviation from the axis of misorientation, $\boldsymbol{l}$, between two adjacent grains supplies a measure of the deviation from exact matching of plane stacks which are nearly normal to $\boldsymbol{l}$ in both grains. This approach to boundary structure has been termed the coincident axial direction (CAD) model [4, 5]. As in the PM model, a CAD boundary can be viewed as a special case of a CSL which is appropriate for large values of Σ, where Σ is the reciprocal density of coinciding lattice points. This equivalence between CSL and CAD/PM for large Σ arises as follows. The three smallest non-coplanar Burgers vectors of grain boundary dislocations in a near-CSL interface define the unit cell of the "displacement shift complete" (DSC) lattice [6]. As Σ increases to about 50 there is considerable anisotropy in the dimensions of the DSC cell. The Burgers vector in the direction parallel to the rotation axis, $\boldsymbol{b}_3$, becomes large in comparison to the other two, $\boldsymbol{b}_1$ and $\boldsymbol{b}_2$, which concurrently diminish. In the limit $\boldsymbol{b}_3$ approaches the interplanar spacing, d, and the DSC cell tends towards a unidimensional form. For example, the $\Sigma = 31$ CSL for fcc has $\boldsymbol{b}_1/\boldsymbol{b}_L = 0.18$ while $\boldsymbol{b}_3/\boldsymbol{b}_L = 0.82$, where $\boldsymbol{b}_L$ is the Burgers vector of a lattice dislocation [6]. For this situation it is both more convenient and physically meaningful to consider misorientations in terms of the CAD rather than the CSL model since matching is now only significant in one dimension, that is along the rotation axis $\boldsymbol{l}$.

0022–2461/88 $03.00 + .12

TABLE I Maximum angular deviations (v_{1m}) and calculated probabilities for CAD rotations $3 < \Pi < 24$ in fcc structures [5]

Π	hkl	v_{1m}	Probability (%)
3	111	11.7	28
4	200	10.1	12
8	220	7.2	16
Total $\Pi = 8$			56
11	311	6.1	
19	331	4.7	
20	420	4.5	
24	422	4.1	
Total $\Pi = 24$			73

The angular range about $\boldsymbol{l}$ over which CADs may be expected to exist in cubic systems can be predicted in a manner analogous to the procedure for CSLs. Because for a CAD interface $\boldsymbol{b}_1$ approaches d, the Burgers vector for a CAD is given by

$$\boldsymbol{b}_{CAD} = a\Pi^{-1/2} \quad (2)$$

where a is the lattice parameter and $\Pi = h^2 + k^2 + l^2$ for rotation axis hkl.

For a CSL,

$$\boldsymbol{b}_{CSL} = \boldsymbol{b}\Sigma^{-1/2} \quad (3)$$

where $\boldsymbol{b}$ is the Burgers vector of primary dislocations in a low-angle boundary. Equations 2 and 3 are proportional to the maximum deviation from an exact CAD or CSL, respectively, which can be accommodated by a DSC lattice. Hence

$$\frac{v_{1m}}{v_{2m}} = \frac{a\Pi^{-1/2}}{\boldsymbol{b}\Sigma^{-1/2}} \quad (4)$$

where v_{1m} and v_{2m} are the CAD and CSL limits, respectively. The commonly accepted dependence of v_{2m} on Σ is [7]

$$v_{2m} = v_0\Sigma^{-1/2} \quad (5)$$

where v_0 is the angular limit for a low-angle boundary.

By substituting for v_{2m} in Equation 4 the expression for the angular limit for a CAD, v_{1m}, is

$$v_{1m} = v_0\left(\frac{a}{\boldsymbol{b}}\right)\Pi^{-1/2} \quad (6)$$

So, for example, v_{1m} for a $\langle 111 \rangle$ CAD in an fcc material is 11.7° [5]. Other values of v_{2m} for $\Pi < 25$ are listed in Table I.

Clearly the angular coverage for CAD boundaries is more extensive than for CSLs and so many more boundaries would be expected to show CAD matching. The fraction of rotations which lie at angles of less than v_{1m} from a CAD have been calculated by Warrington and co-workers from consideration of misorientation "tubes" along CADs in parametral space; details of the procedure are provided in the original publications [4, 5]. Some of the calculated probabilities are included in Table I. For $\Pi < 25$, the prediction is that almost 75% of all boundaries in a randomly oriented polycrystal should possess CAD properties.

The object of the present work is to test the predictions of the CAD model, particularly in comparison with the CSL model, and to assess the implications. Experimentally generated grain-boundary geometrical data from several sources, including that of the authors' own results, has been collated and analysed in terms of deviations from specific CAD axes. The data groups have been chosen so as to represent a cross-section of polycrystalline materials of varying complexity from a pure metal, through a single-phase solid solution alloy, a simple two-phase dispersion-hardened system, a multi-phase steel and finally a complex superalloy. The choice of these groups also serves to illustrate the application of several different microscopical techniques which are suitable for grain-boundary geometrical analysis. Details which pertain to the materials and reference sources are given in Table II [8–13].

2. Experimental procedure

Details of specimen preparation and experimental procedures for all the materials except the austenitic stainless steel are to be found in the references quoted in Table II. The 310 stainless steel specimens were cut from 4 mm thick commercially annealed sheet, mounted in longitudinal section, ground and polished in the normal way and etched in Marble's reagent. The specimens were single-phase solid solution with a uniform grain size of approximately 30 μm. Grain

TABLE II Data sources and relevant information

Sample code	Material	Processing	Experimental technique	Sample size	Ref.
CU	Copper sheet	Cold-rolled 60% annealed 950° C 6 to 7 h	Kossel X-ray diffraction	54	[8]
AS	Austenitic stainless steel Type 310	Cold-rolled and annealed	Electron back-scattered diffraction (EBS)	45	[9]
AL	Al + 0.08% Al_2O_3	Extruded, cold-worked, annealed	Selected-area diffraction	33	[10]
FS	Ferritic stainless steel (E-Brite)	Worked 790° C, quenched and annealed 490° C	Convergent-beam electron diffraction (CBED)	50	[11]
NI	Nickel-based superalloy (Nimonic PE16)	Three experimental heat treatments (see text)	CBED	201	[12, 13]

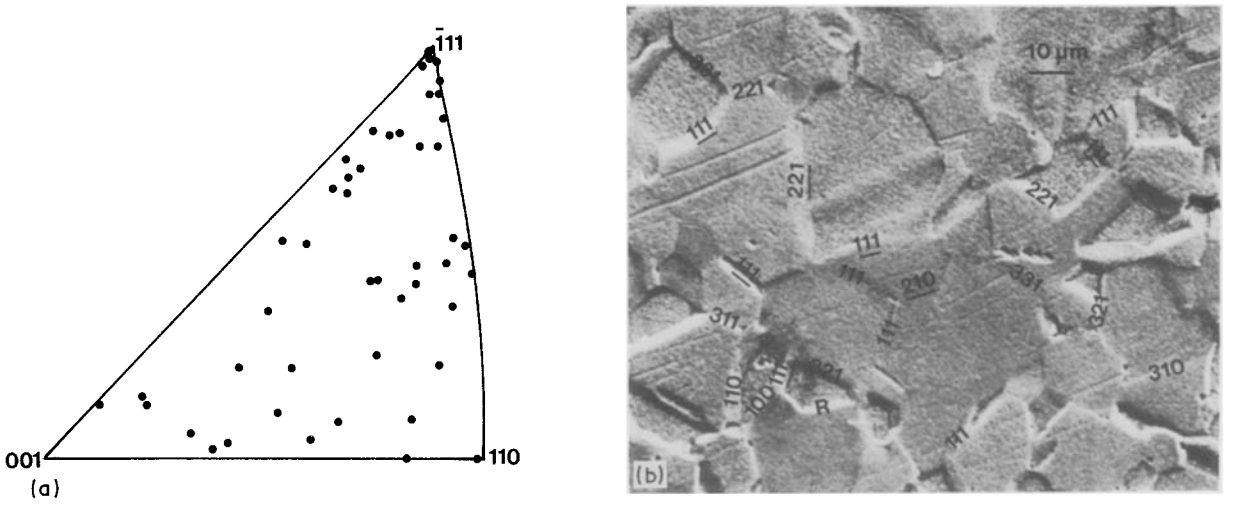

Figure 1 (a) GMT distribution (i.e. plot of rotation axes in a single triangle of the stereographic projection) for the austenitic steel (AS). Some texture near ⟨1 1 1⟩ is apparent. (b) One region from which the boundaries comprising Fig. 1a were sampled. All the boundaries for which misorientation data are available are labelled random (R), or with their CAD axes, or CAD axes underlined, which indicates a CSL.

orientations, and hence axis/angle pairs, l/θ, were acquired by a new technique which exploits the backscattering of electrons (EBS) in a scanning electron microscope. The experimental set-up, and its recent application to the analysis of grain misorientation textures in a superalloy, are described elsewhere [14, 15].

The disorientation between each grain pair (i.e. the lowest-angle solution of the 24 symmetry-related variations for l/θ) [16] was compared to the nearest CAD up to $hkl = 842$ from the following matrix product:

$$M_d = M_e M_c^{-1}$$

where M_d, M_e, and M_c are 3×3 matrices which express the deviation from exact CAD matching, the experimentally obtained disorientation and the exact CAD orientation, respectively. An example will be quoted to make this clear. The nearest CAD axis for a boundary with $l/\theta = 0.982, 0.159, 0.105/33.2°$ is 200. Equation 6 is then used to give the deviation between the experimental l/θ and the exact CAD l/θ, 200/33.2°, which is 6.3°. From the upper limits for the CAD criterion given in Table I, this example is classified as a CAD boundary.

3. Results

The results of the CAD analysis shows that in every case the majority of boundaries, 82 to 91%, are CADs (Table III). When CAD matching is considered for $\Pi \leqslant 8$, that is, ⟨1 1 1⟩, ⟨2 0 0⟩ and ⟨2 2 0⟩ axes only, the CAD frequency is 40 to 49%. There is little intergroup variation (Table III) and in every case the CAD frequency falls short of the predicted value of 56.5% for $\Pi \leqslant 8$ (Table I). The same is true for $\Pi \leqslant 24$.

Table III also includes a breakdown of $\Pi \leqslant 8$ CADs into ⟨1 1 1⟩, ⟨2 0 0⟩ and ⟨2 2 0⟩ subgroups, whereupon textural differences between materials are apparent. To consider first the ⟨1 1 1⟩ sets, the percentage of twin boundaries sampled will affect the number of rotations about this axis. It therefore may be significant that the proportions of twins from each sample correlate approximately with the stacking-fault energy. In the sampling of boundaries from the austenitic steel and superalloy, obvious twin pairs in the microstructure have been avoided. Notwithstanding this bias, the austenitic steel is the only case where the proportion of ⟨1 1 1⟩ CADs (33%) exceeds the theoretical prediction (28%). The distribution of misorientation axes sampled in this material is displayed in Fig. 1a, and the increased density of ⟨1 1 1⟩ poles near the ⟨1 1 1⟩ corner of the unit stereographic triangle is apparent. The authors call this plot the "grain misorientation texture" (GMT) distribution [9, 14]. Fig. 1b is one region from which boundaries were sampled. Random, CAD and CSL boundaries are indicated. Some GMT effects are evident from the clustering of CSLs and to a certain extent similar rotation axes. Similar clustering behaviour has been observed in other systems (e.g. [17]).

The largest divergence between the predicted and actual CAD fraction occurs for the aluminium–alumina alloy. Here the proportion of ⟨2 0 0⟩ CADs (24%) is double that theoretically forecast for the random-texture situation. The fabrication route of the

TABLE III Proportions (%) of CAD boundaries in five different materials. The data in parentheses are twin orientations. hkl refers to the CAD axis and Π is defined in the text. The sample's identity is given in Table I and theoretically derived CAD proportions in Table II

Sample code	CAD $\Pi = 84$	CAD $hkl = 111$	CAD $hkl = 200$	CAD $hkl = 220$	CAD $\Pi = 8$	CAD $\Pi = 24$
CU	85	24(5)	2	15	41	63
AS	91	33(9)	7	9	49	70
AL	89	6(0)	24	9	39	76
FS	82	12(2)	12	20	44	70
NI	87	23(5)	7	12	42	63

material, which involves extrusion and up to 90% cold drawing to wire followed by recrystallization, leads to the promotion of a strong texture, which in this case has influenced the GMT in favour of ⟨2 0 0⟩ CADs. Furthermore, a high proportion of low-angle boundaries is reported, even though primary recrystallization is complete, indicating the presence of a preferred macroscopic texture. The most frequent CAD axis for the low-angle boundaries is ⟨4 2 0⟩, and for high-angle boundaries is ⟨2 0 0⟩. Hence this specimen has a high proportion of $\Pi \leqslant 24$ CADs (76%) and is the only group to exceed the theoretical figure of 72.5%.

To summarize the general implications of the CAD analyses, in general the theory overestimates the CAD fractions. However, the existence of a GMT, whether the direct consequence of overall textural influences (aluminium–alumina alloy) or not apparently linked to grain texture but caused by some boundary misorientation selection process (stainless steel), alters the CAD distributions. The CAD criterion is a convenient way of categorising GMT data.

3.1. Nimonic alloy

Since data from the Nimonic alloy arise from three different heat treatments which have given rise to highly significant microstructural differences, it is instructive in the present context to examine each heat-treatment subgroup separately. It is first necessary briefly to summarize the previous analysis of these data in terms of the CSL model [13] before making a comparison between this and the CAD approach.

The three heat treatments are (a) commercial ageing, so that coherent γ' is precipitated; (b) long overageing, so that γ' coarsens, strongly pinning the boundaries and thus preventing grain growth; and (c) solution treatment of the overaged specimen, so that γ' dissolves and the grain boundaries are able to migrate. When these boundaries were analysed in terms of the CSL model, it turned out that the proportion of CSL boundaries increased from 24 to 47% during overageing, and decreased again when the boundaries migrated during the γ' solution treatment. The interpretation of these results is presented elsewhere [12, 13].

Fig. 2 shows rotation axes of all the grain pairs relative to a single unit triangle of the stereogram. For each heat treatment the CSL boundaries (Figs 2b, d and f) are distinguished from those boundaries which possess only one-dimensional CAD matching (Figs 2a, c and e). A comparison of Figs 2a and b with Figs 2c and d reveals firstly the progression towards a higher CSL fraction as a consequence of overageing, and secondly the avoidance of CADs which are close to the low-index axes ⟨1 1 1⟩, ⟨2 0 0⟩ and ⟨2 2 0⟩ (Figs 2a and c) and, for the aged sample, the additional avoidance of CADs with $h = k = 1$ (Fig. 2a). In other words, rotation axes which are situated in these regions are most favourably sited for three-dimensional CSL matching. This is not a surprising result since almost half of the CSLs with $\Sigma < 49$ (lowest-angle solutions) are misoriented around the three lowest-index rotation axes. Turning now to an examination of shifts in the GMT which result from grain boundary migration when the overaged alloy is reannealed (Figs 2e and f), it is clear that CADs near ⟨2 0 0⟩ and ⟨4 2 0⟩ have become less preferred, and that ⟨1 1 1⟩ CSLs are also disfavoured. Presumably these non-selections have occurred on the grounds of boundary mobility, and the inference is that CSLs misoriented about ⟨1 1 1⟩ do not possess high mobility.

Fig. 3 presents the CAD/CSL data in a manner which not only shows the CAD/CSL GMT distribution but also the proximity to exact matching, via the normalized deviation parameter v_1/v_{1m} or v_2/v_{2m}, where v is the angular deviation of the boundary from the nearest CAD (v_1) or CSL (v_2). Hence not only does the overaged group show an increase in CSLs, but its CAD boundaries have lower values of v_1/v_{1m} than the aged or solution-treated classes (Fig. 3c, cf. Figs 3a and b). But the most striking information contained in Fig. 3 is the complete absence of any ⟨2 0 0⟩ CADs. Any boundaries which are misoriented around this axis are CSLs. This observation is supported by an EBS examination of material which has undergone the overageing treatment and again reveals an extremely small occurrence of ⟨2 0 0⟩ CADs. As yet no obvious explanation for this behaviour can be offered.

4. Discussion

With the advent of such techniques as electron channelling, EBS and CBED it has become possible to approach the topic of preferred orientations from a microtextural (i.e. grain-specific) standpoint (e.g. [14]). The picture which is emerging indicates that often a GMT exists which may be simply related to the grain texture, or in the more complex case may be selected by such boundary characteristics as mobility, solute segregation and precipitation. These effects are being studied in a series of investigations [18, 19]. The usefulness of the CAD approach, especially in conjunction with the CSL model, as a tool for assessment of GMTs, has been demonstrated here.

The results presented here show that almost all boundaries can be defined as CADs. However, whether there are any "special" properties associated with the matching of planes where $4\,2\,2 < hkl < 8\,4\,2$ has not been determined, but it seems unlikely. It is more probable that the observation that 63 to 76% of boundaries are $\Pi \leqslant 24$ CADs has some bearing on boundary properties. Particularly, it lends support to the hypothesis that a totally disordered boundary structure is not a favoured state, and it would therefore follow that structure-sensitive properties such as diffusivity, solubility, energy or sliding capacity are not most accurately represented by their respective values for an unstructured boundary. In order to speculate conceptually how CAD boundary structure could be related to properties, first a single CAD and CSL zone will be considered. Fig. 4 shows a "parametral sphere" schematic representation of a CAD tube around a rotation axis hkl such that all rotations which fall within the tube are CADs. Also, a sphere of radius v_{2m} which represents a CSL falls

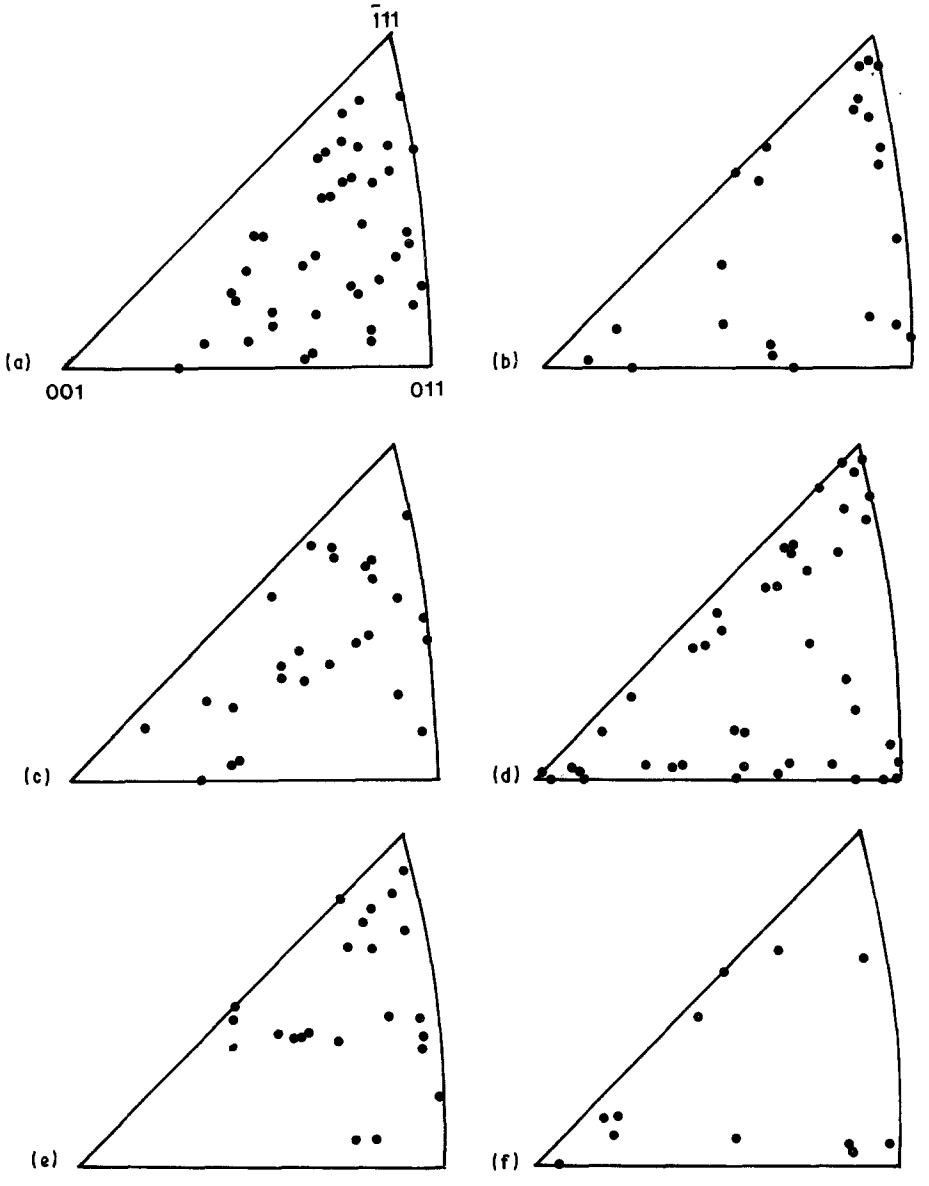

Figure 2 (a–f) GMT distributions for the superalloy (NI) after three different heat treatments: ageing, overageing, and solution treatment. The CSL boundaries (b, d, f) are plotted separately from those boundaries which possess only CAD matching (a, c, e).

within the CAD tube and has been pre-rotated to the origin of the parametral sphere. Since hkl is a unit vector, the radius of the parametral sphere is unity. Each of the loci through the sphere illustrated in Figs 4a to e gives rise to a different structure–property relationship as shown in the accompanying plots (Figs 4f to j). Figs 4b and g depict the case where the structure–property plot passes through the exact CSL configuration, and is identical to the plateau–cusp representation of how grain boundary energy varies with rotation angle (e.g. [20]). However, where the chosen locus through rotation space passes not only through the CSL zone but also through the CAD tube, the structure–property plot must include the effect of the CAD. The modification will be of the kind shown in Figs 4a, c, d and e, that is, a reduction in the height of the plateau region, Δp.

The parametral sphere for cubic crystals does not contain only one CAD tube, but between 63 and 76% of rotation space is covered by CAD zones. Hence the conclusion is reached that the high-energy (or other property) plateau concept of non-CSL boundary structure (Fig. 4g) should be replaced by a series of valleys, mainly shallow in character, so as to include the effect of CAD structure [5].

On the same theme of relaxing the rigorous "structured" or "non-structured" geometrical classification of boundaries, evidence has been published to suggest that any boundary may be represented by a grain-boundary dislocation model, provided the dislocations' Burgers vectors are sufficiently large [21]. It is unlikely that in the foreseeable future this hypothesis can be substantiated from TEM observations of boundaries, because of instrumental resolution limits. Consequently the phenomenological rationale for boundary structure analysis adopted here, namely the statistical analysis of large data sets in terms of their CAD and CSL geometries, offers the most readily available route to gaining a better understanding of the causes and effects of matching at grain boundaries.

5. Conclusions

1. Grain boundary geometry may be represented by a coincident axial direction (CAD) description, or equivalently, a planar matching approach. The essential feature of a CAD/PM boundary is the

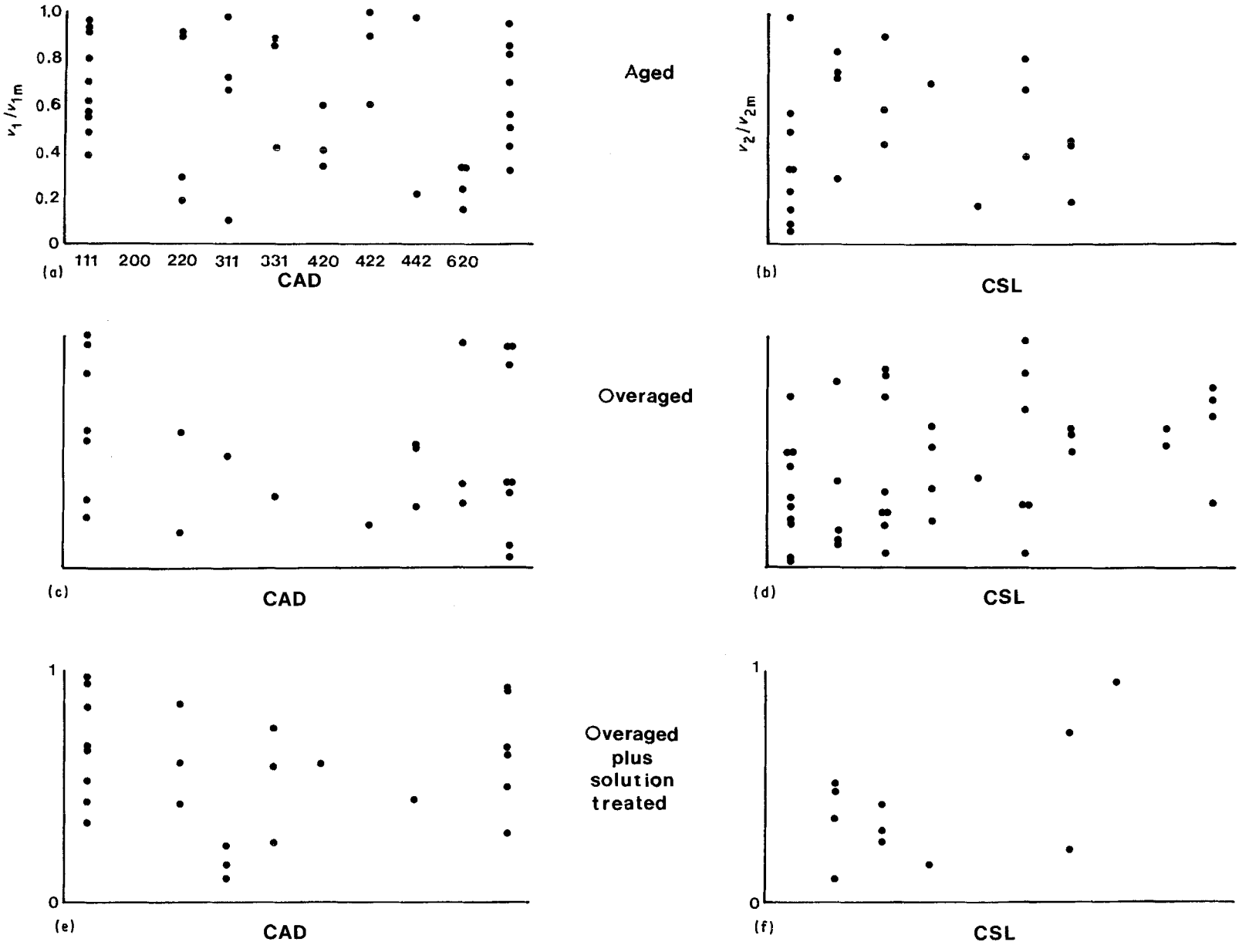

Figure 3 (a–f) Distributions of CAD and CSL rotations in the superalloy (NI) as a function of the normalized deviation parameter from exact matching.

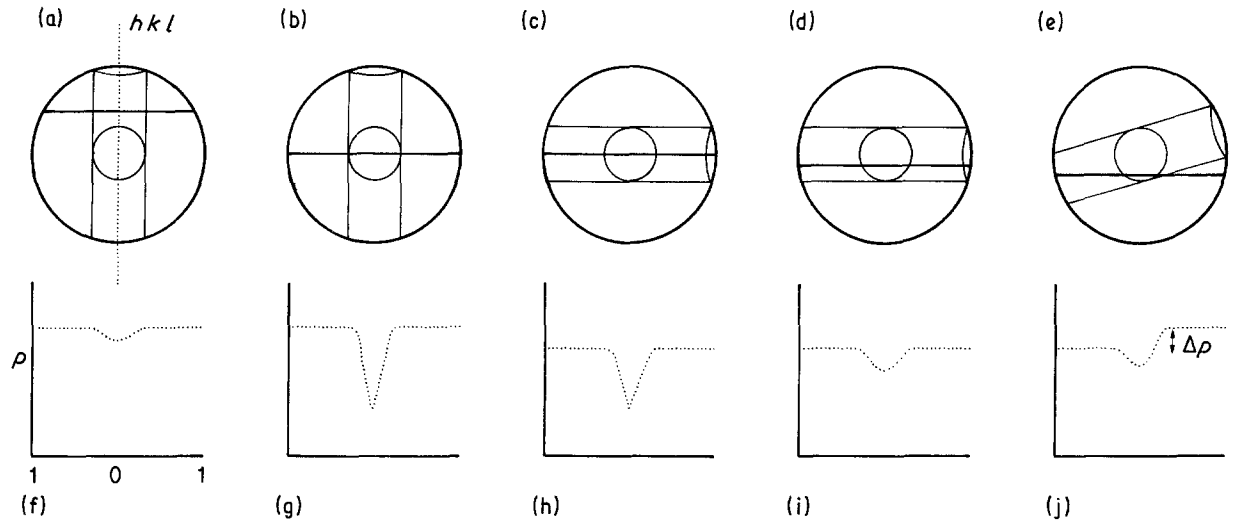

Figure 4 (a–j) Schematic diagrams illustrating how a boundary structure-sensitive property, p, might vary with location in a parametral sphere of unit radius which contains one CSL zone (sphere) and one CAD zone (tube) around rotation axis $h\,k\,l$ where $h\,k\,l$ is a unit vector.

near-parallelism of plane stack normals in each grain, thus allowing linear matching across the boundary.

2. The analysis of several sets of experimentally derived data, representing a range of metals and alloys, reveals that on average 85% of boundaries are CADs with 42% $\Pi \leqslant 8$ and 67% $\Pi \leqslant 24$. The last two proportions are less than the theoretical probabilities for the occurrence of CAD rotations because the theory only accounts for non-textured distributions. In most cases a grain misorientation texture is present, which is made evident by the CAD frequency distribution. Discussion of the GMTs' origins shows that they are either the cause or the result of grain texture.

3. Comparisons between CAD and CSL analyses have been examined for the largest data set. The distribution of CAD axes changed as a function of heat treatment, thus confirming the presence of GMTs in this alloy. The analysis also shows that $\langle 1\,1\,1\rangle$ CSLs are low-mobility orientations and that all the boundary misorientations around axes close to $\langle 2\,0\,0\rangle$ were CSLs.

4. The evidence presented here that 63 to 67% of boundaries possess significant CAD ordering lends support to the view that periodicity, in terms of a general fit/misfit model, exists in most boundaries. The implication is therefore that many boundaries are characterized by different structure-sensitive properties (such as diffusivity, energy, etc.) to those associated with a totally disordered boundary.

Acknowledgements

Permission to publish this paper from the UKAEA, the CEGB and the SSEB is acknowledged. One of us (V.R.) is grateful to the SERC for financial support through a research fellowship. The authors would also like to thank Dr David Warrington for his assistance and advice.

References

1. M. DECHAMPS, F. BARBIER and A. MARROUCHE, *Acta Metall.* **35** (1987) 101.
2. B. RALPH, P. R. HOWELL and T. F. PAGE, *Phys. Status Solidi (b)* **507** (1973) 5.
3. P. H. PUMPHREY, "Grain Boundary Structure and Properties", edited by G. A. Chadwick and D. A. Smith (Academic, New York, 1976) p. 139.
4. D. H. WARRINGTON, *J. Microsc.* **102** (1974) 301.
5. D. H. WARRINGTON and M. BOON, *Acta Metall.* **23** (1975) 599.
6. Y. ISHIDA and M. McLEAN, *Phil. Mag.* **35** (1977) 603.
7. D. G. BRANDON, *Acta Metall.* **14** (1966) 1479.
8. M. LUNNON, PhD thesis, University of Bristol (1979).
9. B. RALPH and V. RANDLE, "Mechanics and Mechanisms of Plasticity" *J. de Physique* (Aussois, Paris, France, 1987) in press.
10. C. J. TWEED, B. RALPH and N. HANSEN, *Acta Metall.* **32** (1984) 1407.
11. H. O. MARTIKAINEN and V. K. LINDROOS, *ibid.* **33** (1985) 1223.
12. V. RANDLE and B. RALPH, in Proceedings of 7th Risø International Symposium on Metallurgy and Materials Science, Risø National Laboratory, Denmark, 1986 (Risø Press, Roskilde) p. 507.
13. *Idem, J. Mater. Sci.* **22** (1987) 2535.
14. V. RANDLE, B. RALPH and D. J. DINGLEY, *Acta Metall.*, in press.
15. V. RANDLE and B. RALPH, work in preparation.
16. *Idem*, in Proceedings of EMAG '85, International Physics Conference Series No. 78 (Adam Hilger, Bristol, 1985) p. 59.
17. P. R. HOWELL, D. E. FLEET, P. I. WELCH and B. RALPH, *Acta Metall.* **26** (1978) 1499.
18. V. RANDLE and B. RALPH, *Proc. Roy. Soc.* (*a*), in press.
19. T. WATANABE, *Res. Mechanica* **11** (1984) 47.
20. P. J. GOODHEW, in Proceedings of EMAG '85, International Physics Conference Series No. 78 (Adan Hilger, Bristol, 1985) p. 155.
21. R. W. BALLUFFI and T. Y. TAN, *Scripta Metall.* **6** (1972) 1033.

Received 10 April
and accepted 29 June 1987